Steel and Composite Structures, *Vol. 36, No. 4* (*2020*) *463-480*
DOI: https://doi.org/10.12989/scs.2020.36.4.463

Ductile crack initiation evaluation in stiffened steel bridge piers under cyclic loading

Wataru Fujie[1], Miki Taguchi[1], Lan Kang[2,3**], Hanbin Ge[*1] and Bin Xu[4,5]

[1]*Department of Civil Engineering, Meijo University, Nagoya 468-8502, Japan*
[2]*School of Civil Engineering and Transportation, South China University of Technology, Guangzhou, Guangdong Province, 510641, People's Republic of China*
[3]*State Key Laboratory of Subtropical Building Science, South China University of Technology, Guangzhou, Guangdong Province, 510641, People's Republic of China*
[4]*College of Civil Engineering, Huaqiao University, Xiamen, Fujian 361021, People's Republic of China*
[5]*Key Laboratory for Intelligent Infrastructure and Monitoring of Fujian Province (Huaqiao University), Xiamen, Fujian 361021, People's Republic of China*

(*Received April 15, 2019, Revised July 15, 2020, Accepted July 17, 2020*)

Abstract. Although detailed shell analysis is suitable to predict the ductile crack initiation life of steel members, such detailed method adds time expense and complexity. In order to simply predict the ductile crack initiation life of stiffened steel bridge piers, a total of 33 cases are simulated to carry out the parametric analyses. In the analysis, the effects of the width-to-thickness ratio, slenderness ratio, plate thickness and so on are considered. Both shell analyses and beam analyses about these 33 cases are conducted. The plastic strain and damage index obtained from shell and beam analyses are compared. The modified factor β_s is determined based on the predicted results obtained from both shell and beam analyses in order to simulate the strain concentration at the base corner of the steel bridge piers. Finally, three experimental results are employed to verify the validity of the proposed method in this study.

Keywords: stiffened steel bridge pier; ductile crack initiation; evaluation method; cyclic loading

1. Introduction

A fracture process composed of ductile crack initiation followed by stable crack growth and finally explosive failure in a ductile mode was observed in the damage of steel members, such as steel beam-to-column connection, steel bridge pier corner, steel brace and so on, as shown in Fig. 1. It is because of the past earthquakes that the failure mode induced by ductile fracture is deemed to be another big problem in thick-walled structures, together with failure mode induced by local buckling occurring in thin-walled structures. As reported by many researchers, the fracture in the steel bridge structures most often occurs at the corner of steel beam-to-column connection and steel bridge pier where stress and strain concentrations provide a ductile trigger to a ductile fracture (Kuwamura and Yamamoto 1997, Ge and Kang 2012, Ge *et al.* 2012, Kang and Ge 2012, Ge *et al.* 2013, Jia *et al.* 2014a; Ahmad *et al.* 2015, Gao *et al.* 2016, Bellahcene and Aberkane 2017, Liu *et al.* 2019). Many researchers focus on the ductile crack initiation, propagation and final failure of structural steels (Kanvinde and Deierlein 2008, Kanvinde *et al.* 2008, Fell *et al.* 2009, Jia and Kuwamura 2013, Boissonnade *et al.* 2014, Jia *et al.* 2014b, Jia and Kuwamura 2014, Khandelwal and El-Tawil 2014, Kiran and Khandelwal 2014b, Kiran and Khandelwal 2014a, Kang *et al.* 2015, Kiran and Khandelwal 2015, Jia *et al.* 2016a, Jia *et al.* 2016b, Kang *et al.* 2016, Wang *et al.* 2016, Kang *et al.* 2018, Fakoor *et al.* 2019). However, because the weld connection details (for example notch, imperfection, heat affect zone) are not easy to be simulated in a structural component model, how to apply these models in a structural member still is a puzzle, yet not to be effectively resolved.

Another effective method is the prediction approach combining the Miner's rule and Manson-Coffin's relationship, in which the damage index is introduced (Liu *et al.* 2005, Tateishi *et al.* 2007). The authors developed a series of evaluation methods to predict the ductile crack initiation life of steel members. The development procedure of ductile crack initiation evaluation method undergoes from shell-level to beam-level (as shown in Fig. 2), and from complex prediction and simplified prediction. First of all, a detailed damage-indexed evaluation method (DDIM) using shell finite element model (abbreviated as shell model) was proposed to evaluate the ductile crack initiation life (Ge and Kang 2012), in which the ductile crack initiation life of seventeen steel members with unstiffened and stiffened cross sections were predicted using the DDIM based on shell model analysis. In addition, a simplified damage-indexed evaluation method (SDIM) was developed to evaluate the ductile crack initiation of steel structures for practical significance and usefulness to actual design using fiber beam model (Ge and Luo 2011), in which a

*Corresponding author, Dr. Eng.
E-mail: gehanbin@meijo-u.ac.jp
**Corresponding author, Ph.D.
E-mail: ctlkang@scut.edu.cn

ISSN: 1229-9367 (Print), 1598-6233 (Online)

Fig. 1 Photos of crack of steel members in lab and practical engineering

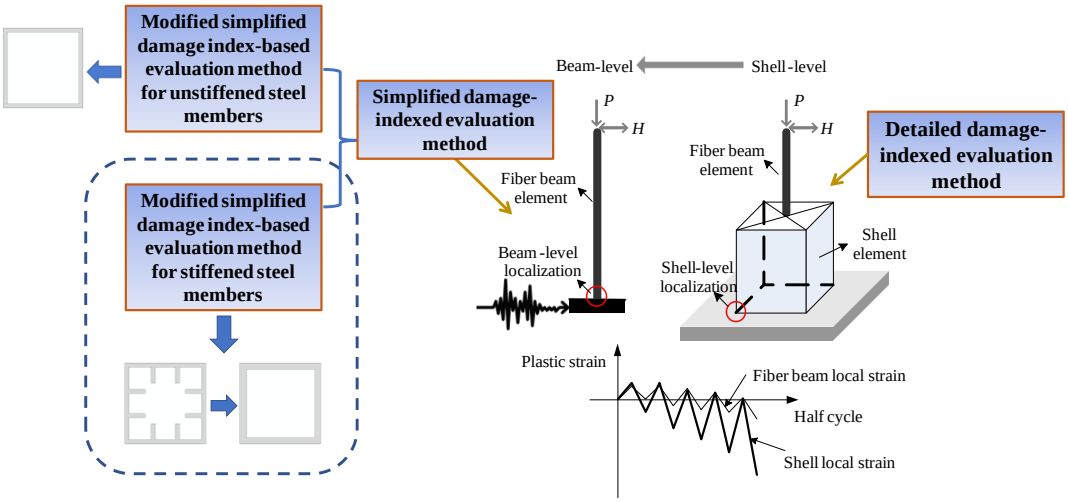

Fig. 2 Mechanism of strain localization from shell-level to beam-level

modification factor β is introduced to magnify plastic strain range obtained from fiber beam model analysis to simulate the strain concentration effect in shell model analysis. For steel bridge piers with unstiffened cross section, a modified simplified damage-indexed evaluation method (MSDIM) was proposed in the reference (Kang and Ge 2015), in which the effects of width-to-thickness ration, slenderness ratio, plate thickness are considered to simulate the strain concentration at steel bridge pier's corner. However, the modified equation obtained in the reference (Kang and Ge 2015) cannot be employed for the steel bridge piers with stiffened cross section because different geometry can lead to different degree of plastic strain concentration.

The focus of this paper is to investigate the evaluation method of the ductile crack initiation of steel bridge piers with stiffened cross section. To this end, this study extends the previous research on the evaluation method to simulate ductile crack initiation using fiber beam model from steel bridge piers with unstiffened cross section to those with stiffened cross section. First of all, this study begins with a brief literature review of previous ductile crack initiation evaluation methods proposed in our previous references (Ge and Luo 2011; Ge and Kang 2012; Ge *et al.* 2013; Kang and Ge 2015). And then, parametric analyses about width-to-thickness ratio, slenderness ratio, plate thickness were carried out. The relationships between modified parameter and width-to-thickness ratio, slenderness ratio, plate thickness are built up based on the parametric analytical results. Finally, the proposed evaluation method in this study was validated based on experimental results of three stiffened steel members.

2. Previous damage index-based evaluation methods

2.1 Formulation of the detailed damage index-based evaluation method (DDIM)

ELCF fracture occurs at large inelastic strain and is driven by complex fracture-fatigue interaction mechanisms that are closely associated with ductile crack initiation. In

the conventional low cycle fatigue (LCF) regime, Manson (1954) and Coffin (1954) independently proposed the following empirical fatigue life relationship that is referred to as the Manson-Coffin relation

$$\varepsilon_p \cdot \left(N_f\right)^k = C \tag{1}$$

where ε_p and N_f are the plastic strain amplitude and the number of cycles to failure, respectively; k and C are material constants. Eq. (1) is represented by a linear relation on the log-log coordinates of ε_p and N_f. Besides, the damage accumulation for LCF under random loading history is based on the Miner's rule (1945). This method assumes that the effect of each cycle is independent, and the damage index D_i is defined as $n_i/N_{f,i}$, where n_i and $N_{f,i}$ are the number of cycles and fatigue life for the i^{th} strain amplitude, respectively. In engineering practice, the cumulative damage index D is equal to zero when there is no damage and is equal to unity when crack initiation occurs. The cumulative damage parameter D is expressed as follows

$$D = \sum D_i = \sum \left(\frac{n_i}{N_{f,i}} \right) = 1.0 \tag{2}$$

Combining Eqs. (1) and (2), the damage indication D can also be expressed as follows (Ge and Kang 2012)

$$D = C' \sum \left(\varepsilon_{pr,i} \right)^m \tag{3}$$

where $\varepsilon_{pr,i}$ is the plastic strain range of i^{th} half cycle, the constants C' and m are calculated through nonlinear regression on unstiffened box steel columns conducted by Ge *et al.* (2009; 2012). Regarding to this method, the plastic strain range instead of the plastic amplitude (half of the plastic strain range) is employed to evaluate the ductile crack initiation because the plastic strain range is not constant during cyclic loading history of practical structures. From the view of the structural level, the constants of Eq. (3) are dependent on not only steel material type but also cross-section, weld toe, heat affected zone and so on. For this evaluation method, these effects are coarsely incorporated in the material constants.

2.2 Formulation of the simplified damage index-based evaluation method (SDIM)

As described in the previous section, ELCF evaluation using the DDIM requires finite element simulations of shell model, which add expense and complexity to the assessing process. With the aim toward developing a simplified damage index-based evaluation method (SDIM) for practical use that dose not require complex shell finite element simulations, a modification factor β is introduced to magnify plastic strain range obtained from fiber beam model analysis to simulate the strain concentration effect in shell analysis. The modification factor β is to convert the beam local strain (beam-level) to the shell local strain (shell-level) corresponding to fracture. The damage index formulation including β is expressed as follows

$$D = C' \sum \left(\beta \cdot \varepsilon_{pr,i} \right)^m \tag{4}$$

In the previous study, the modification factor β has been coarsely determined (Ge and Luo 2011). For the steel bridge pier with unstiffened and stiffened box sections, β was determined to be 3.73 and 6.90, respectively (Ge and Luo 2011). However, it was investigated in all the cases that the modification factor β varies with different plate width-to-thickness ratios (i.e., 0.25, 0.35) and different column slenderness ratios (0.25-0.45). Very little influence was observed in different cyclic loading patterns and steel types (SS400 and SM490) (Ge and Luo 2011). Consequently more detail investigations of various width-to-thickness ratios and slenderness ratios should be further implemented.

2.3 Formulation of the modified simplified damage index-based evaluation method for unstiffened steel members (MSDIM-U)

Based on the previous experimental and analytical results (Ge and Luo 2011), a relationship is observed between the modification factor β and structural parameters, thus, a linear function is selected to relate structural parameters (such as width-to-thickness ratio R_f, slenderness ratio $\bar{\lambda}$ and plate thickness t) to the modification factor β, according to the following equation

$$\beta = C_1 R_f + C_2 \left(\frac{t}{t_0} \right) + C_3 \bar{\lambda} + C_4 \tag{5}$$

where the parameter t_0 is treated as the basic thickness parameter and is selected to be 9 mm. C_1, C_2, C_3 and C_4 are constants, and based on the parametric results they are determined to be 11.1, 1.18, -1.34 and -0.0751, respectively. The modification factor β_u for unstiffened steel members can be obtained as follows

$$\beta_u = 11.1 R_f + 1.18 \left(\frac{t}{t_0} \right) - 1.34 \bar{\lambda} - 0.0751 \tag{6}$$

The applicable range of the above equation is R_f = 0.25 ~ 0.4, and t/t_0 = 1.0 ~ 3.33, and $\bar{\lambda}$ = 0.3 ~ 0.5.

3. Parametric analysis

In order to develop a closed-form equation to calculate the concentrated plastic strain quantities at the strain concentration zone, a series of shell analyses and fiber beam analyses are conducted by using the general finite-element software ABAQUS (2014), respectively, to determine the constants C_1, C_2, C_3 and C_4 for the modification factor β_s of stiffened steel members. First of all, the simulated cases with different structural parameters should be determined. Based on the practical engineering, a total of 33 simulation cases are carried out, in which 27 simulated cases of

Table 1 Geometric dimensions and structural parameters of analytical specimens (for the cases with the plate thicknesses of 10 mm, 20 mm and 30 mm)

Name of specimen $\bar{\lambda}-R_f-t$	$\bar{\lambda}$	R_f	t, t_s (mm)	α	γ/γ^*	h (mm)	b (mm)	b_s (mm)	$\bar{\lambda}_s$	$\overline{t_f}$ (mm)	$\overline{t_w}$ (mm)	P/P_y	H_y (kN)	δ_y (mm)
30-25-10			10			1,482	339	47		11	15		385	6.69
30-25-20		0.25	20			3,048	687	94	0.149	22	29		1,497	13.59
30-25-30			30			4,573	1,031	141		34	43		3,369	20.39
30-35-10			10			2,101	474	51		11	13		524	9.69
30-35-20	0.30	0.35	20	0.5	3.0	4,322	962	103	0.207	22	27	0.1	2,038	19.67
30-35-30			30			6,483	1,443	154		33	40		4,586	29.50
30-45-10			10			2,720	610	55		11	13		660	12.64
30-45-20		0.45	20			5,594	1,237	110	0.269	22	25		2,564	25.67
30-45-30			30			8,392	1,855	165		33	38		5,768	38.50
40-25-10			10			1,975	339	47		11	15		289	11.89
40-25-20		0.25	20			4,065	687	94	0.149	22	29		1,123	24.16
40-25-30			30			6,097	1,031	141		34	43		2,527	36.24
40-35-10			10			2,801	474	51		11	13		393	17.22
40-35-20	0.40	0.35	20	0.5	3.0	5,762	962	103	0.207	22	27	0.1	1,529	34.97
40-35-30			30			8,644	1,443	154		33	40		3,439	52.45
40-45-10			10			3,626	610	55		11	13		495	22.48
40-45-20		0.45	20			7,459	1,237	110	0.269	22	25		1,923	45.63
40-45-30			30			11,189	1,855	165		33	38		4,326	68.44
50-25-10			10			2,469	339	47		11	15		231	18.58
50-25-20		0.25	20			5,081	687	94	0.149	22	29		898	37.75
50-25-30			30			7,621	1,031	141		34	43		2,021	59.36
50-35-10			10			3,501	474	51		11	13		315	26.91
50-35-20	0.50	0.35	20	0.5	3.0	7,203	962	103	0.207	22	27	0.1	1,223	54.64
50-35-30			30			10,804	1,443	154		33	40		2,752	81.96
50-45-10			10			4,533	610	55		11	13		396	35.12
50-45-20		0.45	20			9,324	1,237	110	0.269	22	25		1,538	71.29
50-45-30			30			13,986	1,855	165		33	38		3,461	106.94

Notes: $\bar{\lambda}$ = slenderness ratio parameter, R_f = width-to-thickness ratio parameter, t = plate thickness, t_s = thickness of stiffeners, α = ratio of distance between diaphragms to flange width (a/b , a = spacing between two transverse stiffeners, b = flange width = B-t), γ/γ^* = stiffness ratio of stiffeners (in which γ = stiffness of longitudinal stiffeners, $\overline{t_f}$ = equivalent flange thickness, $\overline{t_w}$ = equivalent web thickness, h = column height, b_s = stiffener width, B = flange width, D = web width, P/P_y = ratio of axial compression force (where the axial yield force P_y is computed when the full cross section is in plasticity, P is the axial force), H_y = yield horizontal force, δ_y = yield transverse displacement

Table 2Geometric dimensions and structural parameters of analytical specimen (for the cases with the plate thickness of 4 mm)

Name of specimen $\bar{\lambda}-R_f-t$	$\bar{\lambda}$	R_f	t, t_s (mm)	α	γ/γ^*	h (mm)	b (mm)	b_s (mm)	$\bar{\lambda}_s$	$\overline{t_f}$ (mm)	$\overline{t_w}$ (mm)	P/P_y	H_y (kN)	δ_y (mm)
20-25-4	0.20	0.25	4	0.5	3.0	295	136	19	0.149	4.5	5.8	0.1	92	1.19
20-35-4		0.35				560	190	20	0.207	4.4	5.4		126	1.72
30-25-4	0.30	0.25				594	136	19	0.149	4.5	5.8		62	2.68
30-35-4		0.35				840	190	20	0.207	4.4	5.4		84	3.88
40-25-4	0.40	0.25		0.5	3.0	790	136	19	0.149	4.5	5.8		46	4.76
40-35-4		0.35				1,120	190	20	0.207	4.4	5.4		63	6.89

Table 3 Material parameters of structural steels

	E (GPa)	v	σ_y (MPa)	ε_y (%)	ε_{st} (%)	E_{st} (GPa)	σ_u (MPa)	ε_u (%)
Plate thickness less than 16 mm	206	0.3	365	0.17	1.2	6.86	490	25
Plate thickness more than 16 mm	206	0.3	355	0.17	1.2	6.86	490	25

Notes: E = Young's modulus, υ = Poisson's ratio, σ_y = yield stress, ε_y = yield strain, ε_{st} = strain at the onset of strain hardening, E_{st} = initial strain hardening modulus, σ_u = ultimate stress (tension strength), and ε_u = ultimate strain

structural parameters (as listed in Table 1) are selected: $\bar{\lambda}$ =0.3, 0.4, 0.5, R_f=0.25, 0.35, 0.45, and t = 10 mm, 20 mm, 30 mm; 6 simulated cases of structural parameters (as listed in Table 2) are selected: $\bar{\lambda}$ =0.2, 0.3, 0.4, R_f=0.25, 0.35, and t = 4 mm. Table 3 lists the material parameters of structural steels in this study. The constitutive law of modified uniaxial two-surface model (Shen *et al.* 1995) is employed.

The structural parameters of width-to-thickness ratio and slenderness ratio are determined as follows (Ge *et al.* 2007)

$$R_f = \frac{b}{t}\sqrt{\frac{12\left(1-\nu^2\right)}{4\pi^2 n^2}}\sqrt{\frac{\sigma_y}{E}} \tag{7}$$

$$\bar{\lambda} = \frac{2h}{r}\frac{1}{\pi}\sqrt{\frac{\sigma_y}{E}} \tag{8}$$

where b = flange width measured from plate thickness centerlines, t = flange thickness, h = column height, n = number of subpanels, r = radius of gyration of cross section, E = Young's modulus, ν = Poisson's ratio and σ_y = yield stress. The slenderness ratio of stiffeners is defined as follows (Usami and Ge 1998)

$$\bar{\lambda}_s = \frac{1}{\sqrt{Q}}\frac{a}{r_s}\frac{1}{\pi}\sqrt{\frac{\sigma_y}{E}} \tag{9}$$

where r_s = radius of gyration of T-shaped cross section and a = spacing between two diaphragms or transverse stiffeners, respectively. And Q stands for the local buckling strength of subpanels surrounded by longitudinal stiffeners, which can be expressed as follows

$$Q = \frac{1}{2R_f}\left[\beta_0 - \sqrt{\beta_0^{\,2} - 4R_f}\right] \le 1.0 \tag{10}$$

$$\beta_0 = 1.33R_f + 0.868 \tag{11}$$

The yield horizontal force H_y and the yield transverse displacement δ_y can be defined as the following equations

$$H_y = \frac{M_y}{0.85h}\left(1-\frac{P}{P_E}\right)\left(1-\frac{P}{P_u}\right) \tag{12}$$

$$\delta_y = \frac{H_y h^3}{3EI} \tag{13}$$

in which M_y = yield moment of cross-section; P_E = Euler's buckling load of a cantilever column; P_u = ultimate strength of a centrally loaded column. The material parameters of structural steel SM490Y used in this study are listed in Table 3. Cyclic loading pattern employed in this study is illustrated in Fig. 3.

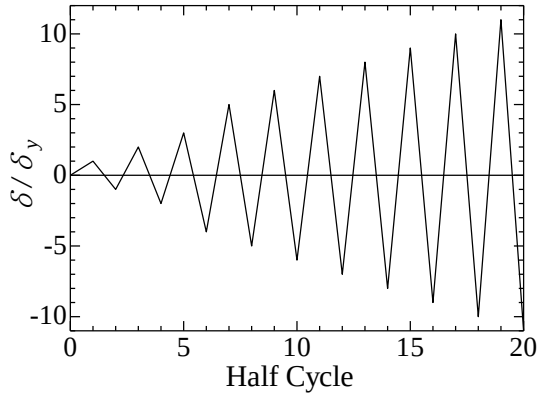

Fig. 3 Cyclic loading pattern employed in this study

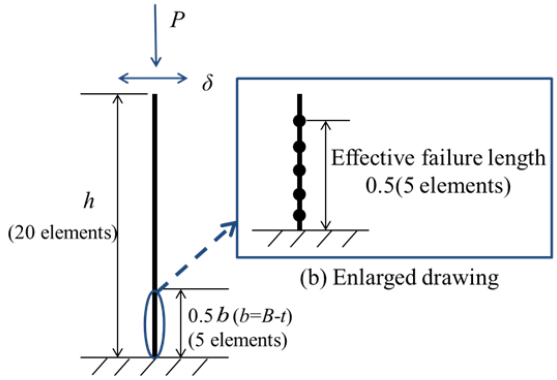

Fig. 4 Beam model

(a) Stiffened cross section (b) Equivalent unstiffened cross section

Fig. 5 Cross section

3.1 Beam model employed in this study

The beam model employed in this study is shown in Fig. 4. The total column was modeled using the fiber beam element of B31 which is based on Timoshenko beam theory. As shown in Fig. 4 the lower part within effective failure length was divided into five elements, which is used for local buckling and ELCF verification. The upper part was divided into 15 elements, and total were 20 elements. Moreover, as shown in Fig. 5, all of the stiffened cross sections were simplified as the equivalent unstiffened cross sections (Zheng *et al.* 2000), and the equivalent web thickness $\overline{t}_w$ and the equivalent flange thickness $\overline{t}_f$ for these stiffened cross sections are listed in Tables 1 and 2, respectively. Furthermore, each analytical cross section had 16 integration points.

3.2 Shell model employed in this study

The shell model employed in this study is shown in Fig. 6. The 4-node reduced integrated shell element of S4R was employed for simulating the 3*a* lower part of the steel column specimen. The upper part of column was modeled using the beam-column element of B31 based on Timoshenko beam theory. To accurately investigate and simulate local buckling and ductile crack initiation in detail, the local meshing around the corner of column-base plate

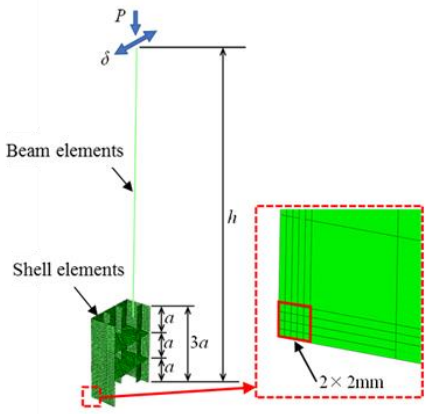

Fig. 6 Shell model

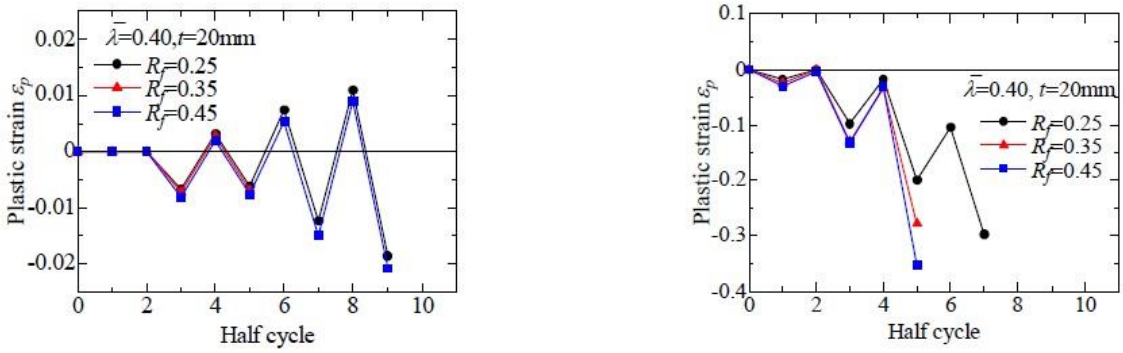

(a) Beam analysis (b) Shell analysis

Fig. 7 Plastic strain history (Effect of R_f)

weld needed to be refined, and the minimum size of refined meshing shell element was 2 mm × 2 mm, as shown in Fig. 6. Because of symmetry, only one-half model of the length of the tested specimens was created. The model was loaded in displacement control. The stiffened cross section for the lower part (shell element part) and the equivalent unstiffened cross section for the upper part (beam element part) of the analytical steel bridge piers were employed.

4. Analytical results and discussions

4.1 Comparison of analytical results between beam model and shell model

In this study, the ductile crack initiation life is depending on the ductile crack initiation life prediction results obtained from shell model. For the shell model, the damage index *D* is calculated by substituting the plastic strain range obtained into Eq. (3). And the ductile crack initiation is predicted when the calculated damage index *D* reaches 1.0. The plastic strain histories obtained from beam model until the ductile crack initiation life obtained from shell model should be output in order to determine the modification factor of stiffened steel bridge piers.

4.1.1 Comparison of plastic strain histories obtained from beam and shell analyses

The plastic strain histories of the cases with $\bar{\lambda} = 0.30$, t = 20 mm, and $R_f = 0.25, 0.35, 0.45$ obtained from beam and shell analyses are illustrated in Fig. 7. The positive part denotes the tension plastic strain and the negative part means the compression plastic strain. It is observed that the cumulative plastic strain increases in compression with the increase in half cycle number regardless of different width-to-thickness ratios and different analytical types. This phenomenon is due to the effect of axial compression force. However, it is demonstrated that the increase of plastic strain in compression for the shell analysis is obviously greater. For example, the plastic strain in compression of the shell analysis at the third half cycle is -0.13, however, that of the beam analysis is about -0.0081, which is greatly smaller than that of shell analysis.

The plastic strain histories of the cases with $\bar{\lambda} = 0.30$, $R_f = 0.35$, and t=4, 10, 20, 30 mm obtained from the beam and shell analyses are illustrated in 0. The difference between the beam analytical cases with different plate thicknesses, as shown in 0 (a), cannot be observed, but the plastic strain of shell analysis obviously increases in compression with the increase in the plate thickness.

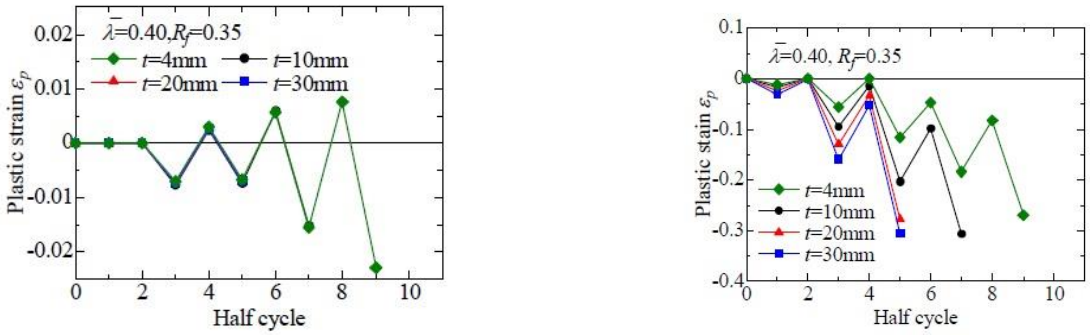

(a) Beam analysis (b) Shell analysis

Fig. 8 Plastic strain history (Effect of *t*)

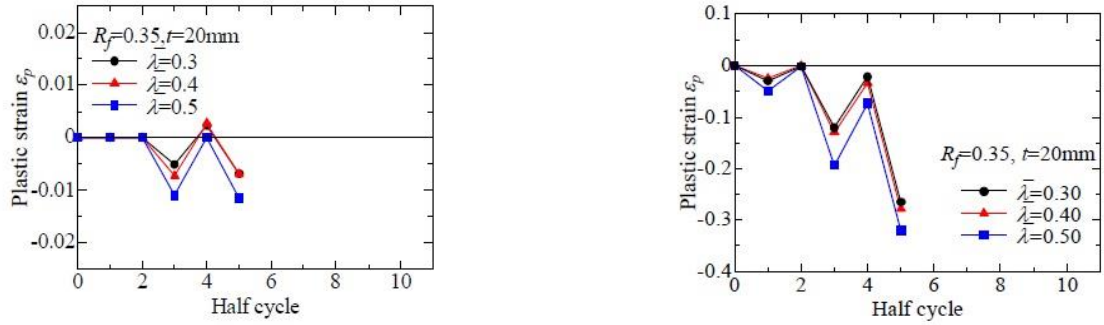

(a) Beam analysis (b) Shell analysis

Fig. 9 Plastic strain history (Effect of $\bar{\lambda}$)

The plastic strain histories of the cases with $R_f = 0.35$, t = 20 mm and $\bar{\lambda} = 0.30, 0.4, 0.5$ obtained from the beam and shell analyses are illustrated in 0. It is found out that the plastic strains of both beam and shell analyses obviously increase in compression with the increase in the slenderness ratio $\bar{\lambda}$.

In summary, the plastic strain obtained from beam analysis is greatly less than that obtained from shell analysis. The analytical results of beam analysis cannot reflect the strain concentration at the base corner of the steel bridge piers. It is very difficult to calculate the damage, which leads to ductile crack initiation, using the beam analysis because the beam model cannot simulate the strain concentration at the base corner of the steel bridge piers.

4.1.2 Comparison of damage index histories obtained from beam and shell analyses

The damage index histories obtained from the beam and shell analyses are demonstrated in Figs. 10-12, in which the damage index histories obtained from the shell analysis are calculated based on Eq. (1).

The ductile crack initiation point is defined as the point at which the damage index D reaches 1.0. It is illustrated that the damage index of all shell analyses reaches 1.0 although the damage index increases with the increases in the width-to-thickness ratio, plate thickness and slenderness ratio, however, the damage index obtained from the beam analysis is very small, and is almost equal to zero. It is concluded that the damage induced by the plastic strain concentration cannot be reflected in the beam analysis.

4.2 Determination of modification factor

The plastic strain histories are obtained through the beam and shell analyses, respectively. The plastic strain ranges in the two analyses are compared, and the ratios of the plastic strain range of the shell analysis to that of the beam analysis are calculated every half cycle, as listed in Table 4. Based on the result of the shell analysis, the predicted ductile crack initiation life is 7 half cycles, and in this case, the parameter β can be calculated by averaging the ratios from the 3rd half cycle to the 7th half cycle. The concentrated plastic strain obtained from the shell analysis is more or less influenced by structural parameters, however similar phenomenon is not obvious during beam analysis, the concentrated plastic strain is not greatly affected by varying structural parameters in beam analysis. Consequently, the modification factor β should reflect the effect of structural parameters on the concentrated plastic strain, and is treated as a structure-dependent damageability coefficient.

4.2.1 Effect of width-to-thickness ratio

Shown in Fig. 13 are plots of β versus the width-to-thickness ratio for the steel bridge piers with slenderness

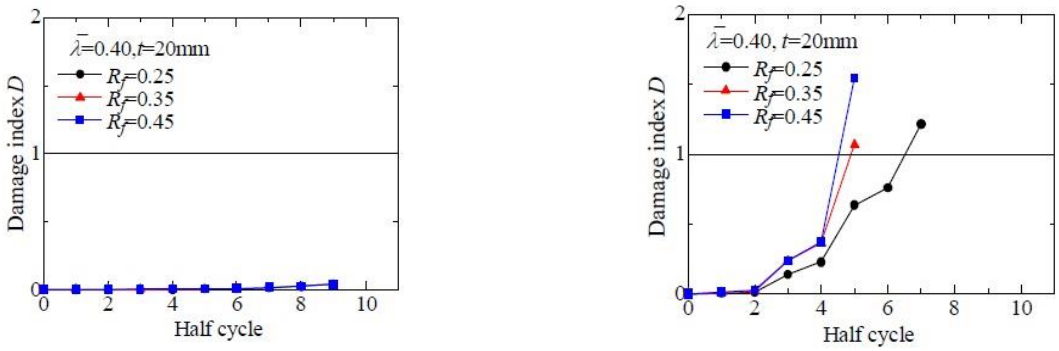

(a) Beam analysis (b) Shell analysis

Fig. 10 Damage index history (Effect of $\bar{R}_f$)

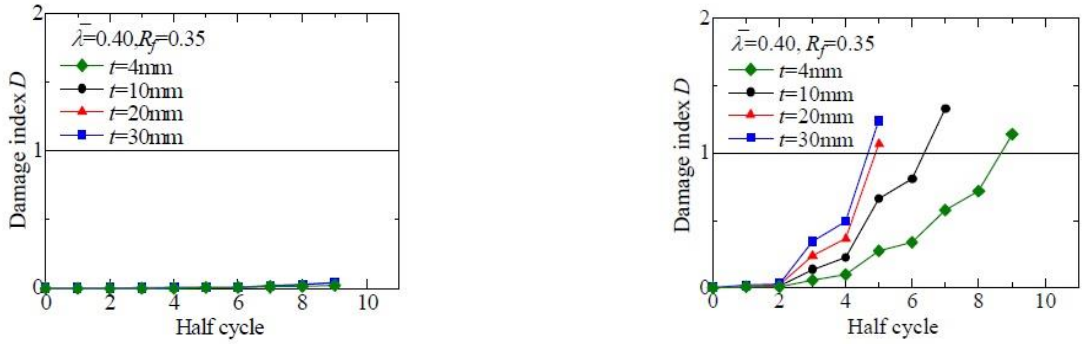

(a) Beam analysis (b) Shell analysis

Fig. 11 Damage index history (Effect of *t*)

Table 4 Comparison of $\varepsilon_{pr,shell}$ and $\varepsilon_{pr,beam}$ (Case 40-25-20 in Table 1)

Half cycle number	$\varepsilon_{pr,shell}$	$\varepsilon_{pr,beam}$	$\varepsilon_{pr,shell}/\varepsilon_{pr,beam}$	Average value
0	0.000	0.000	-	
1	0.019	0.000	-	
2	0.019	0.000	-	
3	0.098	0.007	14.6	11.8
4	0.080	0.010	8.1	
5	0.182	0.009	19.6	
6	0.096	0.014	7.1	
7	0.193	0.020	9.8	

Notes: $\varepsilon_{pr,shell}$ = plastic strain range obtained from shell analysis, $\varepsilon_{pr,beam}$ = plastic strain range obtained from beam analysis

ratio of 0.3, 0.4 and 0.5. The linear regression lines that associate β and width-to-thickness ratio demonstrate a strong correlation between them. This parametric study showed that the modification factor β depends strongly on the width-to-thickness ratio R_f. The slope of curves of the cases with $\bar{\lambda}$ of 0.5 is relatively less than that of curves of the cases with $\bar{\lambda}$ of 0.3 and 0.4. The phenomenon is due to that the plastic strain concentration at the base corner relatively decreases because of such thin-walled and long steel bridge pier. The ductile crack initiation point is delayed because of such steel bridge piers.

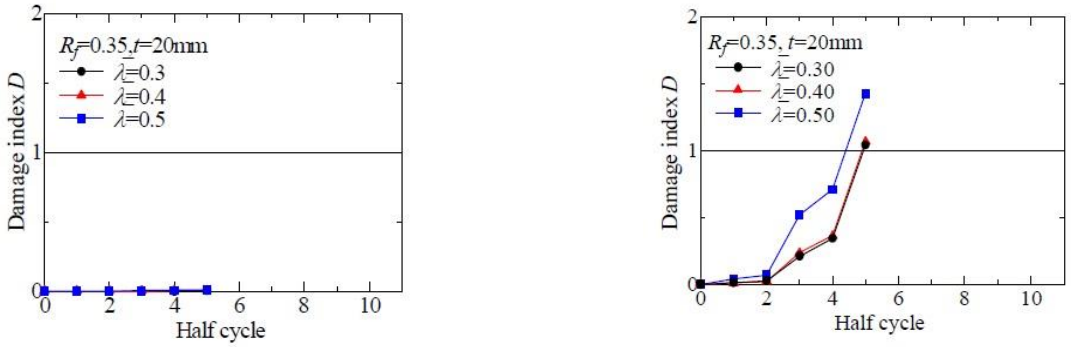

(a) Beam analysis (b) Shell analysis

Fig. 12 Damage index history (Effect of $\bar{\lambda}$)

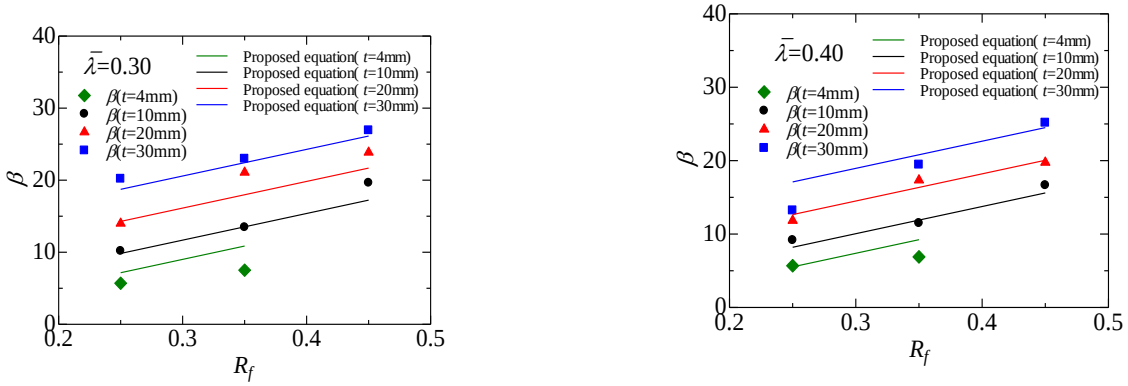

(a) $\bar{\lambda} = 0.30$ (b) $\bar{\lambda} = 0.40$

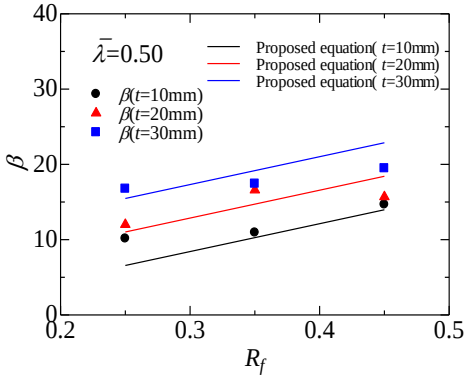

(c) $\bar{\lambda} = 0.50$

Fig. 13 Relationship curves between modification factor and width-to-thickness ratio

4.2.2 Effect of plate thickness

Shown in 0 are plots of β versus the plate thickness ratio for the steel bridge piers with slenderness ratio of 0.3, 0.4 and 0.5. The linear regression lines that associate β and plate thickness ratio demonstrate a strong correlation between them. This parametric study showed that the modification factor β depends strongly on the plate thickness t. Similarly, the slope of curve of the case with $\bar{\lambda}$ of 0.5 and R_f of 0.45 relatively less than that of other curves because of such thin-walled and long steel bridge pier.

4.2.3 Effect of slenderness ratio

The plots of β versus the slenderness ratio for the steel bridge piers with plate thickness of 10 mm, 20 mm and 30 mm are shown in Fig. 15. However, a little decrease of the strain concentration is observed when the column slenderness ratio increases, as illustrated in Fig. 15, because of the P-Δ effect. Meanwhile, the slope of curves of the cases with R_f of 0.45 is relatively less than that of the cases with R_f of 0.25 and 0.35 because ductile crack initiation more easily occurs in the cases with small R_f and local buckling more easily occurs in the cases with large R_f.

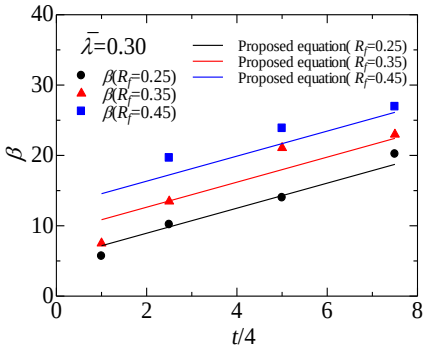

(a) $\bar{\lambda} = 0.30$

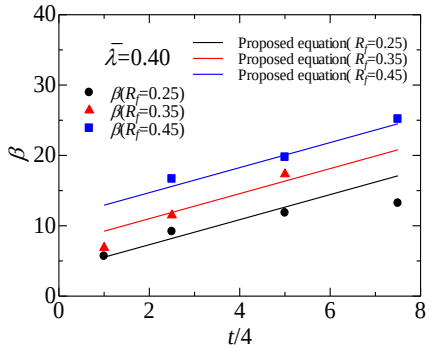

(b) $\bar{\lambda} = 0.40$

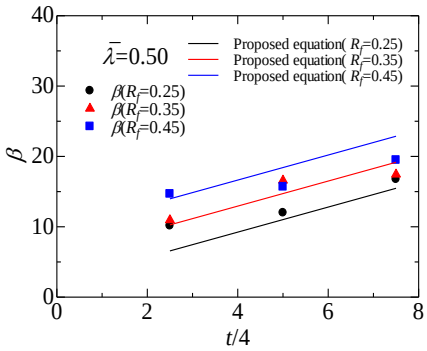

(c) $\bar{\lambda} = 0.50$

Fig. 14 Relationship curves between modification factor and plate thickness

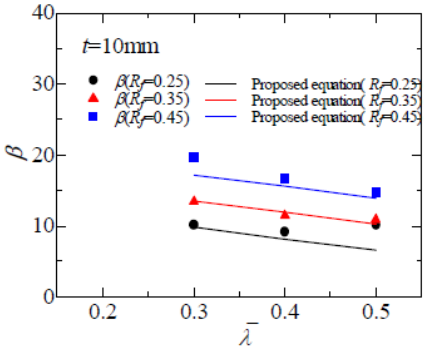

(a) t = 10 mm

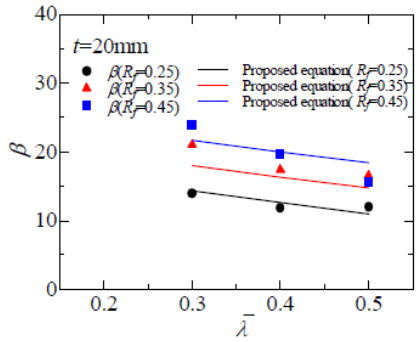

(b) t = 20 mm

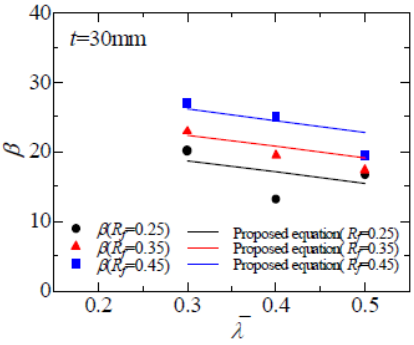

(c) t = 30 mm

Fig. 15 Relationship curves between modification factor and slenderness ratio

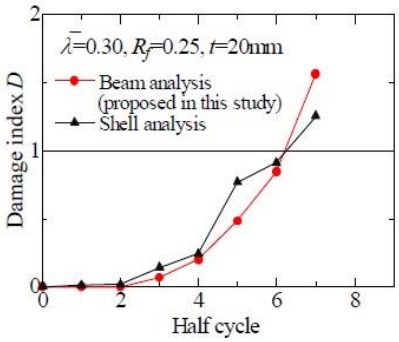

(a) 30-25-20

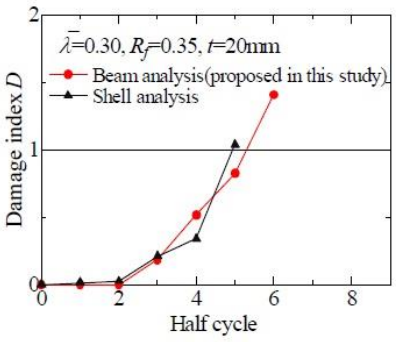

(b) 30-35-20

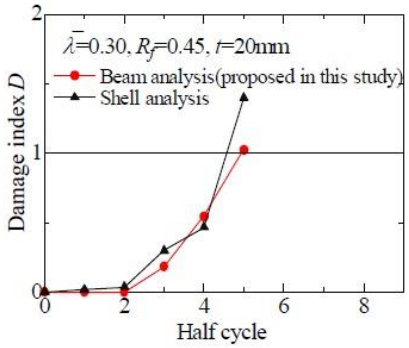

(c) 30-45-20

Fig. 16 Comparison of prediction results obtained from beam analysis using proposed method in this study and shell analysis ($\bar{\lambda}$ = 0.30, R_f = 0.25 ~ 0.45, t = 20 mm)

4.3 Formulation of the modified simplified damage index-based evaluation method for stiffened steel members (MSDIM-S)

Similar calculation processes are conducted for each of the analytical cases to determine all the four constants in the calculation equation of β by the least mean square method from the analytical results. Finally, the modification factor β_s for stiffened steel members can be obtained as following equation based on the parametric analytical results

$$\beta_s = 37.0R_f + 1.78\left(\frac{t}{4}\right) - 16.3\bar{\lambda} + 1.02 \qquad (14)$$

The applicable range of above equation is R_f = 0.25 ~ 0.45, and t = 4 ~ 30 mm, and $\bar{\lambda}$ = 0.2 ~ 0.5. The cases which exceed this range should be verified by more analytical and experimental investigations. The damage index formulation including β_s employed for stiffened steel bridge piers is expressed as follows

$$D = C'\sum\left(\beta_s \cdot \varepsilon_{pr,i}\right)^m \qquad (15)$$

4.4 Calibration of the proposed method in this study

4.4.1 Comparison of predicted results obtained from beam analysis using proposed method in this study and shell analysis

In order to verify the validity of the proposed method in this study, the beam analyses employing the proposed method in this study are carried out. The comparison of prediction results obtained from the beam analysis using the proposed method in this study and shell analysis is shown in Figs. 16-18. Taking the case of 30-35-20 as one example as shown in Fig. 16(b), the ductile crack initiation life obtained from the shell analysis is 5 half cycles, and that obtained from the beam analysis employing the proposed method in this study is 6 half cycles, which is only one half cycle more than shell analytical result. It is demonstrated that the difference between the ductile crack initiation life predicted by the shell analysis and that predicted by the beam analysis using the proposed method in this study is equal to or less 1 half cycle. It is concluded that the ductile crack initiation life predicted by the beam analysis using the proposed method in this study agrees well with that obtained from the shell analysis.

Fig. 19 illustrates the total comparison of predicted results obtained from the beam analysis using the proposed method in this study and shell analysis. In which, $H.C._{dci,pre}$ is the half cycle number of ductile crack initiation life predicted by the beam analysis based on the proposed method in this study, and $H.C._{dci,shell}$ is the half cycle number of ductile crack initiation life predicted by the shell analysis. ±20% prediction error boundaries are also plotted. It is obviously observed from Fig. 19 that most data

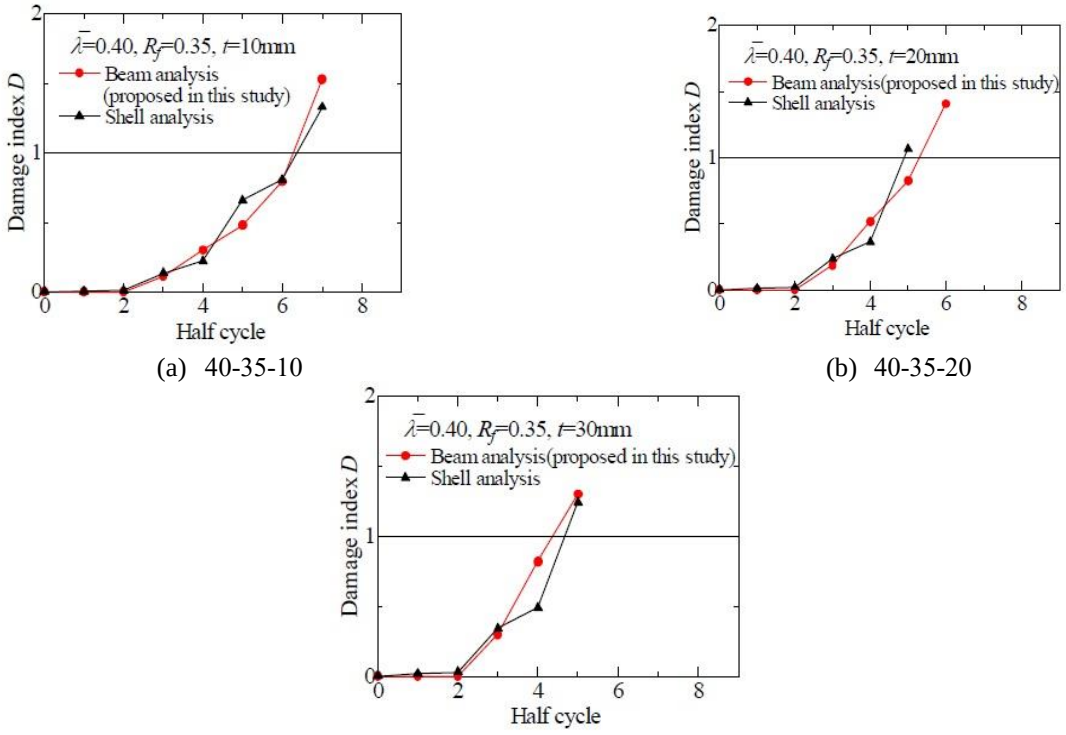

(a) 40-35-10 (b) 40-35-20

(c) 40-35-30

Fig. 17 Comparison of prediction results obtained from beam analysis using proposed method in this study and shell analysis ($\bar{\lambda}$ = 0.40, R_f = 0.35, t = 10 ~ 30 mm)

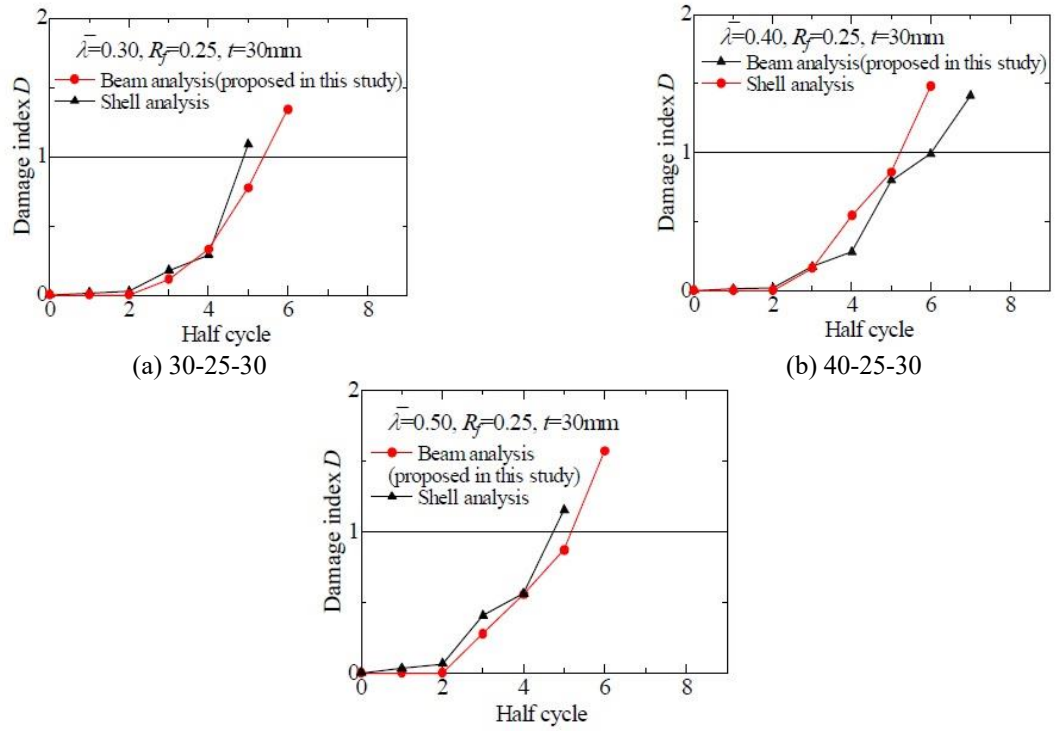

(a) 30-25-30 (b) 40-25-30

(c) 50-25-30

Fig. 18 Comparison of prediction results obtained from beam analysis using proposed method in this study and shell analysis ($\bar{\lambda}$ = 0.30 ~ 0.50, R_f = 0.25, t = 30 mm)

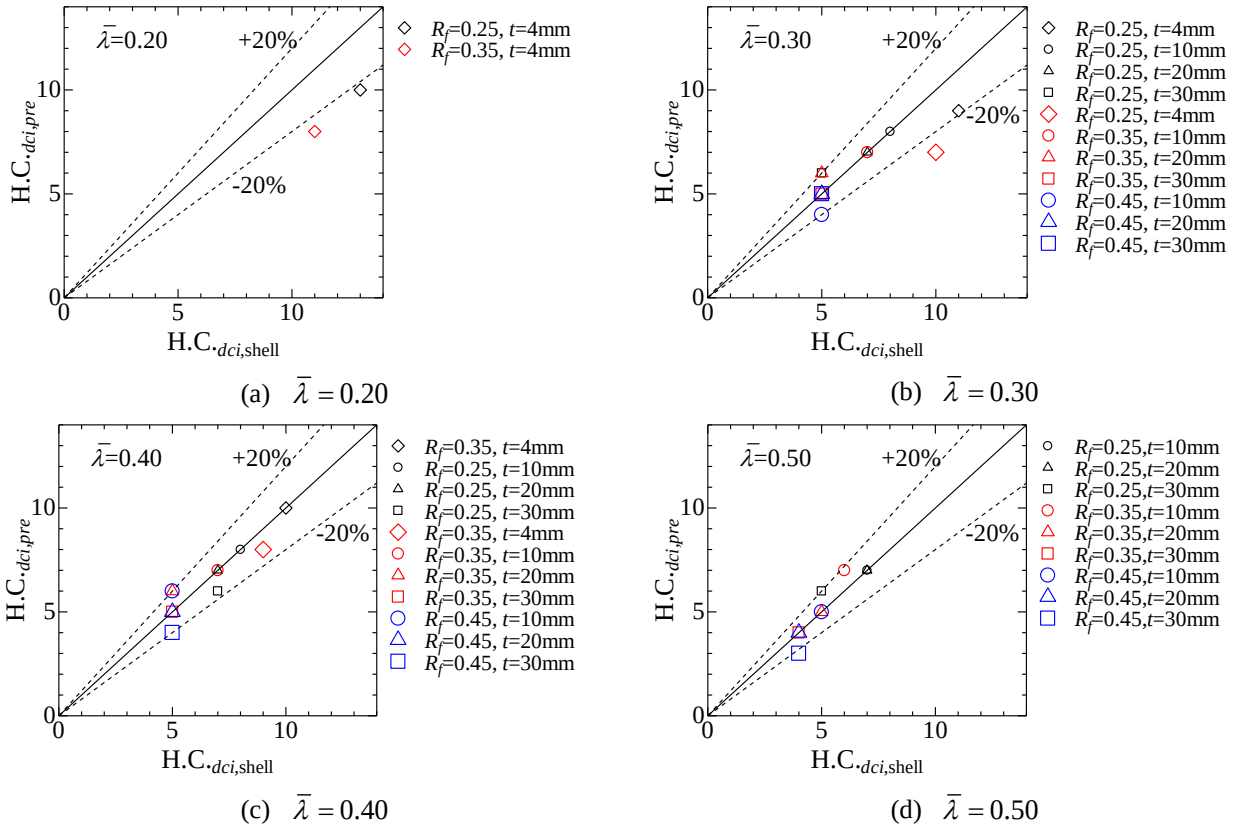

Fig. 19 Comparison of prediction results obtained from beam analysis using proposed method in this study and shell analysis

points lie within the ±20% margin lines. The maximum prediction error in this study is -30%, and this relatively large prediction error occurs in the case with the plate thickness of 4 mm. However, such prediction error can be acceptant in practical engineering. Consequently, the prediction results employing the beam analysis based on the proposed method in this study show good agreement with those using the shell analysis.

4.4.2 Comparison of predicted results obtained from beam analysis using proposed method in this study and tested results

In order to verify the validity of this proposed method, the predicted results obtained from the beam analysis using the proposed method in this study are compared with the experimental results of S35-35I (Yoshizaki *et al.* 1999), KD-10 (Nakamura *et al.* 1997) and NCF20 (Lawson and Saverirajan 2011). The geometric dimensions and structural parameters of tested specimens are listed in 0, and the material parameters of structural steels of tested specimens are listed in Table 6. A comparison of the prediction results obtained from the beam analysis using the proposed method in this study and the experimental results is shown in Fig. 20. For the SM490 steel, C = 9.69 and m = 1.86; for the SM400 steel, C = 8.23 and m = 1.82 (Ge and Luo 2011, Ge and Kang 2012).

In which, the predicted result of KD-10 is 8 half cycles equal to the tested result, the predicted result of S35-35I is 7 half cycles less than the tested result of 10 half cycles, and the predicted result of NCF20 is 5 half cycles less than the tested result of 7 half cycles. The prediction error of S35-35I and NCF20 is -30% and -29%, respectively. Such prediction error is similar to the maximum prediction error (-30%) in the cases with the plate thickness of 4 mm in section 4.4.1. The plate thickness of S35-35I and NCF20 is 4.9 mm and 4.5 mm, respectively, and then the prediction error of them is similar to the prediction error in the case with the plate thickness of 4 mm. However, the prediction error of KD-10 is very small, which's plate thickness is 10 mm. It is concluded that the prediction results obtained from the beam analysis based on the proposed method in this study show good agreement with the tested results, especially for the cases with the plate thickness of 10 ~ 30 mm, and the proposed method in this study can be employed in the ductile crack initiation life of steel members in practical engineering.

The verification of the proposed method in tests is very limited because of only three ductile fracture tests of stiffened steel bridge piers subjected to cyclic loading. More stiffened steel bridge pier tests should be carried out to verify the applicability of the proposed method in this study. The corresponding experimental research is ongoing.

Table 5 Geometric dimensions and structural parameters of tested specimens

	h (mm)	α	B (mm)	t (mm)	b_s (mm)	t_s (mm)	R_f	$\bar{\lambda}$	P/P_y	H_y (kN)	δ_y (mm)
S35-35I	1033	0.5	224	4.9	26	4.9	0.35	0.35	0.172	99.8	5.6
KD-10	3303	0.5	720	14	90	10	0.35	0.30	0.148	837	13.3
NCF20	745	1.0	200	4.5	22	4.5	0.452	0.241	0.20	93.7	3.77

Tabled 6 Material parameters of structural steels of tested specimens

		Steel type	σ_y (MPa)	E (GPa)	ε_y (%)	E_{st} (GPa)	ε_{st} (%)	σ_u (MPa)	ε_u (%)	v
S35-35I		SM490YA	382	208	0.183	5.05	1.12	574	31	0.275
KD-10	Plate	SM490A	318.7	206	0.1547	6.867	1.083	627	44.48	0.3
	Stiffener		379.9	206	0.1844	5.150	1.844	638.3	40.63	0.3
NCF20		SM400A	338	200	0.169	4.98	1.69	417	27	0.3

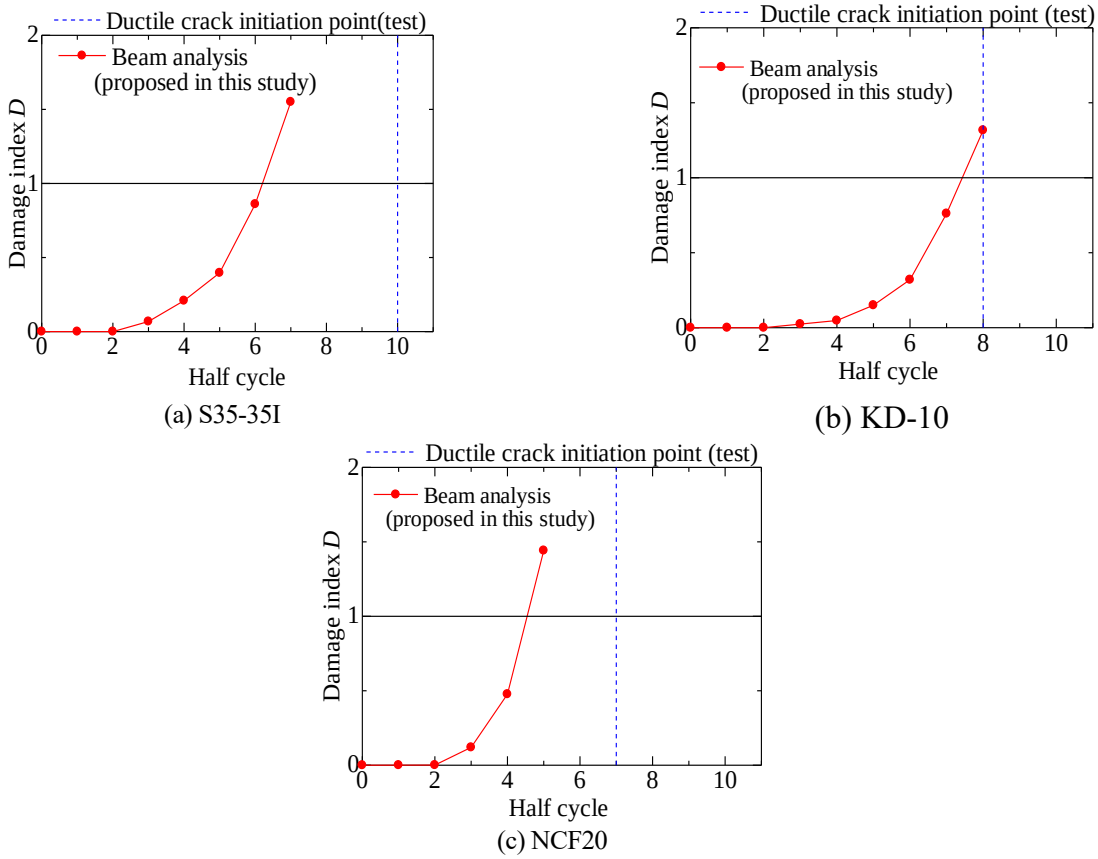

Fig. 20 Comparison of prediction results obtained from beam analysis using proposed method in this study and experimental results

5. Conclusions

A novel simplified prediction method employed for the ductile crack initiation life prediction of stiffened steel members was proposed in this study. A previous detailed damage index-based evaluation method was intended to capture a relationship between the cumulative damage and the strain range of each half cycle. And a previous modified simplified damage index-based evaluation method for unstiffened steel members was proposed for simply predicting the ductile crack initiation life of unstiffened members using the beam model. The purpose of this study is to simply predict the ductile crack initiation life of stiffened steel members.

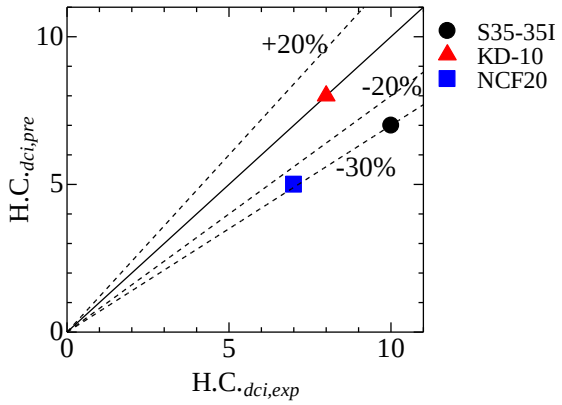

Fig. 21 Comparison of prediction results obtained from beam analysis using proposed method in this study and experimental results

1) A modification factor β_s was proposed in this study to capture the relationship between the strain concentration and the structural parameters of stiffened members. Total 33 parametric analyses were carried out to find out the linear relationships between β_s and the width-to-thickness ratio, plate thickness and slenderness ratio.
2) For the cases with the plate thickness of 10 ~ 30 mm, compared with the shell analytical results, the prediction error of the beam analysis based on the proposed method in this study was within $\pm$20%; for the cases with the plate thickness of 4mm, the prediction error of the beam analysis based on the proposed method in this study was from 0 to -30% compared with the shell analytical results.
3) The prediction results of the proposed method in this study were compared with the tested results. About -30% prediction error occurred in the cases with the plate thickness of 4 ~ 5 mm, and the prediction life was equal to the tested result for the case with the plate thickness of 4 mm.
4) It is concluded that the proposed method in this study is enough accurate for predicting the ductile crack initiation life of stiffened members under cyclic loading suitable for earthquake engineering applications.

It is important to emphasize that the empirical formulas presented in this paper are based on a range of specimen structural parameters which may be commonly encountered in structural engineering. These include the width-to-thickness ratio parameter R_f = 0.25 ~ 0.45, the plate thickness t = 4 ~ 30 mm, and the slenderness ratio parameter $\bar{\lambda}$ = 0.2 ~ 0.5. Since the formulas are semi-empirical, they may require modifications when applied to situations that are not within this range of parameters.

Acknowledgements

The study is supported in part by JSPS KAKENHI Grant Number JP18K04333, the Guangdong province Special Support Program "Innovating Science and Technology for Young Top Talents" (2016TQ03Z528), the Natural Science Foundation of Guangdong Province (2020A1515011070), and the Fundamental Research Funds for the Central Universities (D2191360). The financial supports are highly acknowledged.

References

ABAQUS (2014), *ABAQUS/Analysis User's Manual-version 6.14*, ABAQUS, Inc.: Pawtucket, Rhode Island.

Ahmad, M.I.M., Arifin, A., Abdullah, S., Jusoh, W.Z.W. and Singh, S.S.K. (2015), "Fatigue crack effect on magnetic flux leakage for A283 grade C steel", *Steel Compos. Struct.*, **19**(6), 1549-1560. http://dx.doi.org/10.12989/scs.2015.19.6.1549.

Bellahcene, T. and Aberkane, M. (2017), "Estimation of fracture toughness of cast steel container from Charpy impact test data", *Steel Compos. Struct.*, **25**(6), 639-648. https://doi.org/10.12989/scs.2017.25.6.639.

Boissonnade, N., Nseir, J., Lo, M. and Somja, H. (2014), "Design of cellular beams against lateral torsional buckling", *Proceedings of the Institution of Civil Engineers-Structures and Buildings*, **167**(7), 436-444. https://doi.org/10.1680/stbu.12.00049.

Coffin, Jr. L.F. (1954), "A study of the effects of cyclic thermal stresses on a ductile metal", *T. Am. Soc. Mech. Engineers*, **76** 931-950.

Fakoor, M., Rafiee, R. and Zare, S. (2019), "Equivalent reinforcement isotropic model for fracture investigation of orthotropic materials", *Steel Compos. Struct.*, **30**(1), 1-12. https://doi.org/10.12989/scs.2019.30.1.001.

Fell, B.V., Kanvinde, A.M., Deierlein, G.G. and Myers, A.T. (2009), "Experimental investigation of inelastic cyclic buckling and fracture of steel braces", *J. Struct. Eng. – ASCE*, **135**(1), 19-32. https://doi.org/10.1061/(ASCE)0733-9445(2009)135:1(19).

Gao, Y., Zhou, Z., Liu, D. and Wang, Y. (2016), "Cracking of a prefabricated steel truss-concrete composite beam with pre-embedded shear studs under hogging moment", *Steel Compos. Struct.*, **21**(5), 981-997. https://doi.org/10.12989/scs.2016.21.5.981.

Ge, H.B. and Kang, L. (2012), "A damage index-based evaluation method for predicting the ductile crack initiation in steel structures", *J. Earthq. Eng.*, **16**(5), 623-643. https://doi.org/10.1080/13632469.2012.676231.

Ge, H.B., Kang, L. and Hayami, K. (2013), "Recent research

developments in ductile fracture of steel bridge structures", *J. Earthq. Tsunami*, **7**(3), 1350021. https://doi.org/10.1142/S1793431113500218.

Ge, H.B., Kang, L. and Tsumura, Y. (2012), "Extremely low-cycle fatigue tests of thick-walled steel bridge piers", *J. Bridge Eng. – ASCE*, **18**(9), 858-870. https://doi.org/10.1061/(ASCE)BE.1943-5592.0000429.

Ge, H.B., Kawahito, M. and Ohashi, M. (2007), "Experimental study on ductile crack initiation and its propagation in steel bridge piers of thick-walled box sections", *J. Struct. Eng. - JSCE*. **53A** 493-502.

Ge, H.B. and Luo, X.Q. (2011), "A seismic performance evaluation method for steel structures against local buckling and extra-low cycle fatigue", *J. Earthq. Tsunami*, **5**(2), 83-99. https://doi.org/10.1142/S1793431111001005.

Ge, H.B. and Tsumura, Y. (2009), "Experimental and analytical study on the evaluation of ductile crack initiation in steel bridge piers", *J. Struct. Eng. – JSCE*, **55A**, 605-616.

Jia, L.J., Ge, H. and Suzuki, T. (2014a), "Effect of post weld treatment on cracking behaviors of beam-column connections in steel bridge piers", *Steel Compos. Struct*., **17**(5), 685-702. http://dx.doi.org/10.12989/scs.2014.17.5.685.

Jia, L.J., Ge, H.B., Shinohara, K. and Kato, H. (2016a), "Experimental and numerical study on ductile fracture of structural steels under combined shear and tension", *J. Bridge Eng. – ASCE*, **21**(5), 04016008. https://doi.org/10.1061/(ASCE)BE.1943-5592.0000845.

Jia, L.J., Ikai, T., Kang, L., Ge, H. and Kato, T. (2016b), "Ductile cracking simulation procedure for welded joints under monotonic tension", *Struct. Eng. Mech.*, **60**(1), 51-69. http://dx.doi.org/10.12989/sem.2016.60.1.051.

Jia, L.J., Koyama, T. and Kuwamura, H. (2014b), "Experimental and numerical study of post-buckling ductile fracture of heat-treated SHS stub columns", *J. Struct. Eng. – ASCE*, **140**(7), 04014044. https://doi.org/10.1061/(ASCE)ST.1943-541X.0001056.

Jia, L.J. and Kuwamura, H. (2013), "Prediction of cyclic behaviors of mild steel at large plastic strain using coupon test results", *J. Struct. Eng. – ASCE*, **140**(2), https://doi.org/10.1061/(ASCE)ST.1943-541X.0000848.

Jia, L.J. and Kuwamura, H. (2014), "Ductile fracture simulation of structural steels under monotonic tension", *J. Struct. Eng. – ASCE*, **140**(5), 04013115. https://doi.org/10.1061/(ASCE)ST.1943-541X.0000944.

Kang, L. and Ge, H. (2012), "Strength and ductility evaluation method for steel bridge pier frames considering effect of shear failure", *Adv. Steel Constr.*, **8**(4), 366-382.

Kang, L., Ge, H. and Fang, X. (2016), "An improved ductile fracture model for structural steels considering effect of high stress triaxiality", *Constr. Build. Mater*., **115**, 634-650. https://doi.org/10.1016/j.conbuildmat.2016.04.083.

Kang, L. and Ge, H.B. (2015), "Predicting ductile crack initiation in steel bridge piers with unstiffened box section under specific cyclic loadings using detailed and simplified evaluation methods", *Adv. Struct. Eng*., **18**(9), 1427-1442. https://doi.org/10.1260/1369-4332.18.9.1427.

Kang, L., Ge, H.B. and Kato, T. (2015), "Experimental and ductile fracture model study of single-groove welded joints under monotonic loading", *Eng. Struct*., **85**, 36-51. https://doi.org/10.1016/j.engstruct.2014.12.006.

Kang, L., Suzuki, M., Ge, H. and Wu, B. (2018), "Experiment of ductile fracture performances of HSSS Q690 after a fire", *J. Constr. Steel Res.*, **146**, 109-121. https://doi.org/10.1016/j.jcsr.2018.03.010.

Kanvinde, A.M. and Deierlein, G.G. (2008), "Validation of cyclic void growth model for fracture initiation in blunt notch and dogbone steel specimens", *J. Struct. Eng. –ASCE*, **134**(9), 1528-1537. https://doi.org/10.1061/(ASCE)0733-9445(2008)134:9(1528).

Kanvinde, A.M., Fell, B.V., Gomez, I.R. and Roberts, M. (2008), "Predicting fracture in structural fillet welds using traditional and micromechanical fracture models", *Eng. Struct*., **30**(11), 3325-3335. https://doi.org/10.1016/j.engstruct.2008.05.014.

Khandelwal, K. and El-Tawil, S. (2014), "A finite strain continuum damage model for simulating ductile fracture in steels", *Eng. Fract. Mech.*, **116**, 172-189. https://doi.org/10.1016/j.engfracmech.2013.12.009.

Kiran, R. and Khandelwal, K. (2014a), "Fast-to-compute weakly coupled ductile fracture model for structural steels", *J. Struct. Eng. – ASCE*, **140**(6), 04014018. https://doi.org/10.1061/(ASCE)ST.1943-541X.0001025.

Kiran, R. and Khandelwal, K. (2014b), "A triaxiality and Lode parameter dependent ductile fracture criterion", *Eng. Fract. Mech.*, **128**, 121-138. https://doi.org/10.1016/j.engfracmech.2014.07.010.

Kiran, R. and Khandelwal, K. (2015), "A micromechanical cyclic void growth model for ultra-low cycle fatigue", *Int. J. Fatigue*, **70**, 24-37. https://doi.org/10.1016/j.ijfatigue.2014.08.010.

Kuwamura, H. and Yamamoto, K. (1997), "Ductile crack as trigger of brittle fracture in steel", *J. Struct. Eng. –ASCE*, **123**(6), 729-735. https://doi.org/10.1061/(ASCE)0733-9445(1997)123:6(729).

Lawson, R.M. and Saverirajan, A.H.A. (2011), "Simplified elasto-plastic analysis of composite beams and cellular beams to Eurocode 4", *J. Constr. Steel Res.*, **67**(10), 1426-1434.

Liu, W.C., Liang, Z. and Lee, G.C. (2005), "Low-cycle bending fatigue of steel bars under random excitation. Part II: Design considerations", *J. Struct. Eng. – ASCE*, **131**(6), 919-923.

Liu, Y., Kang, L. and Ge, H.B. (2019), "Experimental and numerical study on ductile fracture of structural steels under different stress states", *J. Constr. Steel Res*., **158**, 381-404.

Luo, X.Q., Ge, H.B. and Ohashi, M. (2012), "Experimental study on ductile crack initiation in compact section steel columns", *Steel Compos. Struct*., **13**(4), 383-396. https://doi.org/10.12989/scs.2012.13.4.383.

Manson, S. (1954), *Behaviour of materials under conditions of thermal stress*, Lewis Flight Propulsion Laboratory, Cleveland.

Miner, M.A. (1945), "Cumulative damage in fatigue", *J. Appl. Mech*., **12**(3), 159-164. ttps://doi.org/10.1007/978-3-642-99854-6_35.

Nakamura, S., Yasunami, H., Kobayashi, B., Nakagawa, T. and Mizutani, S. (1997), "An experimental study on the seismic performance of steel bridge piers with less-stiffened and compact sized section", *Proceedings of nonlinear numerical analysis and seismic design of steel bridge piers*, 331-338.

Shen, C., Mamaghani, I.H.P., Mizuno, E. and Usami, T. (1995), "Cyclic behavior of structural steels. II: Theory", *J. Eng. Mech. ASCE*, **121**(11), 1165-1172. https://doi.org/10.1061/(ASCE)0733-9399(1995)121:11(1165).

Tateishi, K., Hanji, T. and Minami, K. (2007), "A prediction model for extremely low cycle fatigue strength of structural steel", *Int. J. Fatigue*, **29**(5), 887-896. https://doi.org/10.1016/j.ijfatigue.2006.08.001.

Usami, T. and Ge, H.B. (1998), "Cyclic behavior of thin-walled steel structures--numerical analysis", *Thin-Wall. Struct.*, **32**(1-3), 41-80. https://doi.org/10.1016/S0263-8231(98)00027-5.

Wang, P.J., Wang, X.D., Liu, M. and Zhang, L.L. (2016), "Web-post buckling of fully and partially protected cellular steel beams at elevated temperatures in a fire", *Thin-Wall. Struct.*, **98** 29-38. https://doi.org/10.1016/j.tws.2015.02.028.

Yoshizaki, K., Usami, T. and Honma, D. (1999), "Pseudodynamic tests of steel bridge piers with purpose of reducing residual displacements", *J. Struct. Eng. – JSCE*, **45A**, 1017-1026.

Zheng, Y., Usami, T. and Ge, H.B. (2000), "Ductility evaluation procedure for thin-walled steel structures", *J. Struct. Eng. – ASCE*, **126**(11), 1312-1319. https://doi.org/10.1061/(ASCE)0733-9445(2000)126:11(1312).

BU